Scripta Materialia 177 (2020) 69–73

Contents lists available at ScienceDirect

Scripta Materialia

journal homepage: www.elsevier.com/locate/scriptamat

Solute segregation assisted nanocrystallization of a cold-rolled Mg–Ag alloy during annealing

L.R. Xiao[a,b], X.F. Chen[b], Y. Cao[b], H. Zhou[a,b,*], X.L. Ma[c], D.D. Yin[d], B. Ye[e], X.D. Han[a,**], Y.T. Zhu[b,c]

[a] Beijing Key Lab of Microstructure and Property of Advanced Materials, Beijing University of Technology, Beijing 100124, China
[b] Nano and Heterogeneous Materials Center, School of Materials Science and Engineering, Nanjing University of Science and Technology, Nanjing 210094, China
[c] Department of Materials Science & Engineering, North Carolina State University, Raleigh, NC 27695, USA
[d] Key Laboratory of Advanced Technologies of Materials, Ministry of Education, School of Materials Science and Engineering, Southwest Jiaotong University, Chengdu, Sichuan 610031, China
[e] National Engineering Research Center of Light Alloys Net Forming and State Key Laboratory of Metal Matrix Composite, Shanghai Jiao Tong University, 200240 Shanghai, China

ARTICLE INFO

Article history:
Received 3 July 2019
Revised 7 October 2019
Accepted 8 October 2019

Keywords:
Nanocrystalline materials
Mg alloy
Transmission electron microscopy
Interfacial segregation

ABSTRACT

Refining grains to nanoscale has been a challenge, especially for materials with low-melting points and poor ductility, such as Mg alloys. Here we report a novel mechanism of nanocrystallization assisted by solute segregation, by which a nanocrystalline Mg-Ag alloy was produced by moderate cold rolling (~55% strain) followed by low-temperature annealing. Specifically, during cold rolling non-basal $\langle c+a \rangle$ dislocations were activated to form dislocation cells walls, which were pinned by Ag segregation, and transformed into boundaries of nanocrystalline grains during annealing.

Nanocrystallization is an effective strategy to improve strength-to-weight ratios of metallic materials. Materials with high strength-to-weight ratios are attractive for structural applications in which weight is a major concern [1–3]. Plastic deformation has been reported capable of producing nanostructured materials with large dimensions and no porosity [4–7]. However, the plastic strain required for nanocrystallization is much higher than typical applied strains of conventional industrial processing such as rolling, forging and extrusion [8].

Magnesium (Mg) has the lowest density (1.74 g/cm^3) among all commonly known structural metals, and Mg alloys are well known for their high strength-to-weight ratios. However, Mg and its alloys have a hexagonal close-packed (HCP) crystal structure and low melting points. This makes it especially challenging to produce nanostructured materials via plastic deformation. In general, the HCP structure renders a material low and anisotropic plasticity. A Mg alloy with an HCP structure has only two independent easy (basal $(0001)\langle 11\bar{2}0 \rangle$) slip systems at room temperature. According to the Von Mises criterion [9–11], five independent slip systems are required for homogeneous deformation without cracking. Therefore, deformation twinning is often activated to provide additional slip systems in a Mg alloy [6]. However, deformation twins in HCP structures are asymmetric and can induce local stress concentration. Thus, it is difficult to deform Mg and its alloys to high plastic strains, even with the activation of deformation twinning. Consequently, plastic deformation of Mg alloys is usually conducted at an elevated temperature to activate non-basal slip systems such as prismatic and pyramidal slip [12–14]. However, melting points of Mg alloys are usually low, and dynamic recovery and grain growth are readily to occur at elevated temperatures. As a result, grain refinement induced by plastic deformation is limited in Mg alloys at elevated processing temperatures [15,16]. For example, grain sizes of an AM60 Mg alloy produced by equal channel angular pressing at 150, 250 and 350 °C are ~ 1 μm, ~2 μm and ~10 μm, respectively [17]. Clearly, the challenge for producing bulk nanostructured Mg alloys is still in front of us, so an alternative approach is urgently need to tackle it.

A Mg-2.57 wt% Ag alloy was used as a model material in this work. Detailed information on the experimental procedure can be found in the Supplemental materials.

* Corresponding author at: Beijing Key Lab of Microstructure and Property of Advanced Materials, Beijing University of Technology, Beijing 100124, China.
** Corresponding author.
E-mail addresses: hzhou511@njust.edu.cn (H. Zhou), xdhan@bjut.edu.cn (X.D. Han).

https://doi.org/10.1016/j.scriptamat.2019.10.012
1359-6462/

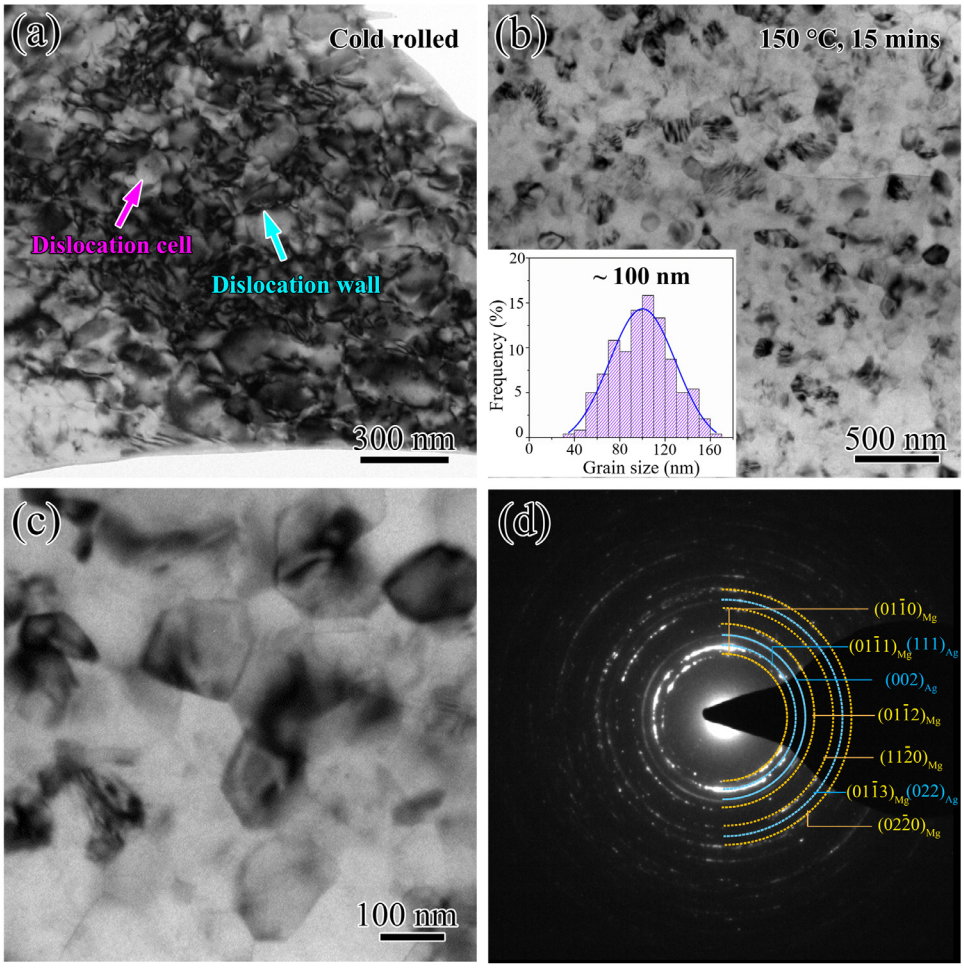

Fig. 1. TEM images of Mg–Ag samples processed by (a) cold rolling, (b) and (c) cold rolling + annealing at 150 °C for 15 mins. The inset in (b) is the grain size histogram. (d) The selected area electron diffraction pattern taken from (b), in which the diffraction rings of Mg and Ag are marked by yellow and blue indexes, respectively.

Fig. 1a reveals a high density of dislocations in the cold rolled Mg–Ag alloy sample. The dislocations are entangled with each other, forming nano-scaled dislocation walls and cells. Interestingly, Fig. 1b shows a nanocrystalline grain structure formed after cold rolling and annealing at 150 °C for 15 mins. Enlarged TEM image in Fig. 1c shows equiaxed nano-grains, whose interiors are nearly defect free. As shown in the inset of Fig. 1b, the grain sizes are in the range of 30–170 nm with an average value of ~ 100 nm. The selected area diffraction pattern (SADP) in Fig. 1d exhibits typical polycrystalline diffraction rings of nanocrystalline materials [18,19]. The rings of both HCP Mg and FCC Ag are observed, indicating that pure Ag phase was precipitated out from the Mg matrix.

It is impossible to produce nanocrystalline structure in pure Mg by cold rolling and annealing, according to literature [20,21]. Thus, it is reasonable to hypothesize that in the Mg–Ag alloy the Ag played a critical role in producing the nanocrystalline structures observed in this work. Due to the clear difference between the atomic numbers of the constituent elements (Mg: 12, Ag: 47), it is easy to detect the heavy Ag atoms by using HAADF-STEM [22–25]. Fig. 2a shows the atomic-resolution HAADF-STEM image of as-received Mg–Ag specimen observed from the $[11\bar{2}0]$ zone axis. The image exhibits a typical solid solution morphology without any solute clustering. After cold rolling, uniformly dispersed nano-scale domains with sizes of 2–3 nm were observed (the bright nano-domains in Fig. 2b), which indicates the formation of Ag-rich clusters. STEM-EDS was conducted on a cold rolled sample in hope of identifying the Ag-rich regions. Unfortunately, the nanoclusters with sizes of 2–3 nm are quickly damaged by electron radiation [26,27]. In order to improve the stability of the clusters, a short time annealing at 150 °C for only 1 min was done to the cold rolled sample to grow the clusters slightly. As shown in Fig. S1, the Ag-rich clusters have grown up to ~5 nm after annealing. Clearly, the center spacing between clusters in both cold rolled sample (Fig. S1a) and annealed sample (Fig. S1b) are nearly identical, indicating that large clusters (Fig. S1b) grew from the small ones (Fig. S1a). As shown in Fig. S1c and d, strong signal of Ag atoms was detected in the clusters, supporting that the clusters with bright contrast shown in Fig. S1a and b are rich of Ag atoms. Enlarged image in Fig. 2c shows a partial dislocation with the Burgers vector of $1/6\langle 2\bar{2}03\rangle$ in the cold rolled sample. Bright contrast at the dislocation core indicates the concentration of Ag atoms. According to literature [28,29], the observed partial dislocation is a result of the dissociation of a $\langle c+a\rangle$ dislocation. Provided that the rolling process was performed at room temperature; Ag clustering occurred due to the low solubility and high diffusion speed of Ag atoms in Mg matrix. In addition, the strain fields associated with dislocations tend to attract Ag atoms, and thus promote segregation of Ag atoms [22,30,31].

A cold rolled Mg-Ag sample was annealed at 150 °C for 5 mins. As shown in Fig. 2d, Ag atoms have segregated along some linear features. TEM analysis was performed at the same position of Fig. 2d. The bright field TEM image and the corresponding selected area diffraction pattern are added as supplemental materials (see

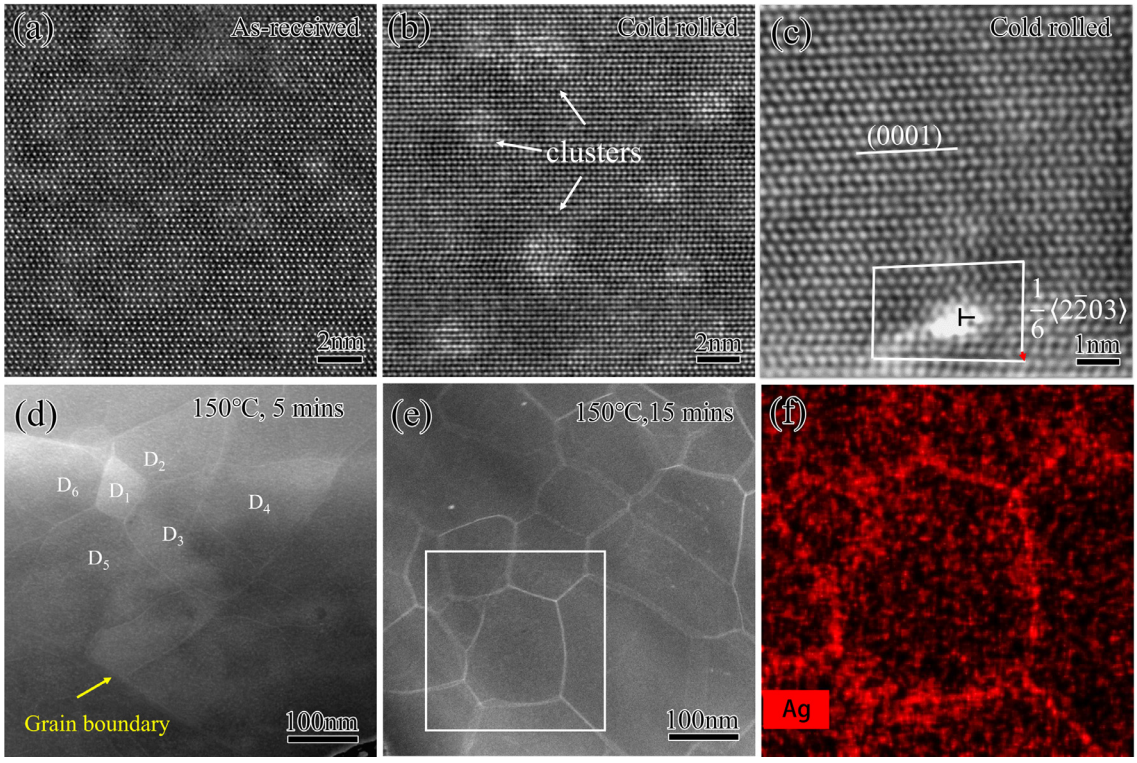

Fig. 2. HAADF-STEM images of Mg–Ag alloy: (a) as-received, (b) and (c) cold rolled, (d) 150 °C, 5 mins, (e) and (f) 150 °C, 15 mins.

Fig. S2). As shown in Fig. S2b, the diffraction spots are sharp and circular, indicating that the linear features enclosed by the yellow circle in Fig. S2a are dislocations rather than low angle grain boundaries. Dislocations in crystalline solids are linear defects, which attract solute segregation when diffusion is enabled [32]. Therefore, diffusion and segregation of Ag atoms towards dislocations clearly have been promoted during the annealing process. As mentioned earlier, partial dislocations and non-basal $\langle c+a\rangle$ dislocations have been widely identified in the cold rolled Mg–Ag sample (Fig. 2c). Cross slip of partial dislocations and non-basal $\langle c+a\rangle$ dislocations strongly assist the formation of dislocation cells. Thus, it is anticipated that the dislocation free regions (Fig. 2d) subdivided by entangled dislocations are underdeveloped dislocation cells with an average size of ~100 nm.

Fig. 2e shows the HAADF-STEM image of the Mg–Ag alloy sample processed by cold rolling and subsequent annealing at 150 °C for 15 mins. As revealed in Fig. 1, homogeneous nanocrystalline structures have formed in this sample. Therefore, equiaxed regions delineated by segregated boundaries are actually equiaxed nanograins. Fig. 2f. is an EDS mapping image of the area enclosed by a rectangle in Fig. 2e, showing strong Ag segregation along the boundaries.

TKD analysis was carried out to characterize the microstructures of the Mg–Ag alloy processed by cold rolling and subsequent annealing at 150 °C for 15 mins, and to help determine the nature of the segregated boundaries shown in Fig. 2e. The TKD results provided in Fig. 3a again support that homogeneous nanocrystalline structures have been achieved in the Mg–Ag alloy. According to the statistical result of the grain size distribution provided in Fig. 3b, the Mg–Ag alloy sample has a grain size distribution of 40–190 nm and an average size of ~103 nm. Clearly, the grain sizes measured by the TKD method is nearly identical to those measured by TEM (Fig. 1b). In addition, information about misorientations at boundaries can be extracted from the TKD results [33]. As shown in Fig. 3a, the microstructure of the Mg–Ag alloy sample consists of large domains delineated by high-angle grain/domain boundaries (HAGBs) and nano-grains delineated by low-angle grain boundaries (LAGBs). Five typical domains can be identified in Fig. 3a, and the domain boundaries are traced by blue lines. The boundaries in Domains I, II and III are numbered and analyzed in detail. Interestingly, boundaries at the interior of the domains are all LAGBs with angles of misorientation less than 15°, and the domain boundaries are all HAGBs with angles of misorientation greater than 15°. For example, as shown in Fig. 3c, the grain boundaries inside the Domain I, numbered from 1 to 14, are all LAGBs (<15°); In contrast, the boundaries surrounding the domain, numbered from 15 to 35, are all HAGBs (>15°). The same results are obtained for Domain II and III, as shown in Fig. 3d and e.

Based on abovementioned experimental results, a solute segregation assisted grain refinement mechanism is proposed and schematically illustrated in Fig. 4. At the beginning, the Mg–Ag alloy was a coarse-grained solid solution containing a low density of crystalline defects (Fig. 4a). The sample was firstly processed by rolling. Due to the low solubility of Ag in the Mg–Ag alloy at low temperatures (Fig. S3), and under the effect of rolling strain, a high density of Ag-rich clusters (2–3 nm) nucleated at the interior of the coarse grains. Ag-rich clusters (represented by the red spots in Fig. 4b) can effectively impede dislocation slip and increase the dislocation storage capability [6]. Therefore, a high density of dislocations (as represented by the blue lines in Fig. 4b) including large amounts of partial and non-basal dislocations was generated and entangled to accommodate the plastic strain. The cold rolled sample was then annealed at a certain temperature. As illustrated in Fig. 4c, net-like dislocation structures, which formed due to the cluster pinning effect and dislocation entanglement, subdivided the coarse grains into nanostructures. Once the annealing process began, Ag atoms quickly segregated along the dislocation lines of the entangled dislocations, as evidenced by the dislocation net with bright-contrast in Fig. 2d. With sufficient annealing time, significant amounts of Ag atoms segregated to the dislocation boundaries. Dislocation boundaries are non-equilibrium boundaries with excess amounts of dislocations. As Ag atoms segregate

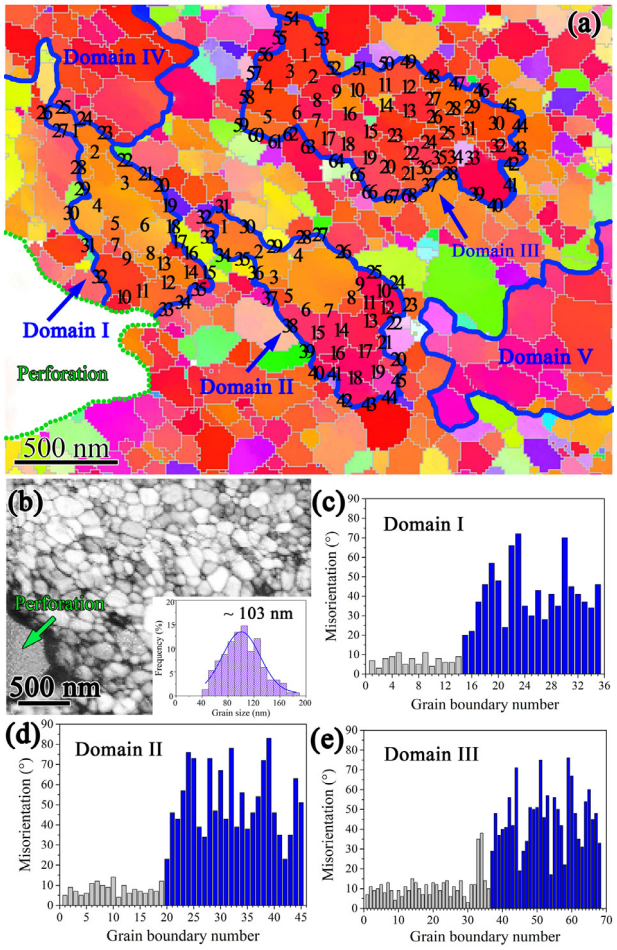

Fig. 3. TKD analysis of the Mg–Ag alloy sample processed by cold rolling and subsequent annealing at 150 °C for 15 mins: (a) a TKD mapping image, (b) the corresponding band contrast image of (a), and (c)–(e) histograms of boundary misorientations in Domains I, II and III. (HAGBs are traced by blue lines and LAGBs are traced by gray lines.).

to the dislocation boundaries, the dislocation boundaries are gradually restructured and the misorientations of the boundaries are gradually increased. Eventually, the dislocation boundaries were transformed into LAGBs that subdivided the coarse grains into equiaxed nano-grains as illustrated in Figs. 1, 3 and 4d. Similar to most of nanocrystalline metals, the nano-grain Mg–Ag alloy is also in a metastable intermediate state, and its long-term stability is worthy to be studied further.

Ag solute and its segregation were found to play a critical role in assisting the grain nanocrystallization process. Firstly, in the solid solution of Mg–Ag, non-basal $\langle c \rangle$ and $\langle c+a \rangle$ dislocation systems are activated during cold rolling. However, under the same cold rolling condition, the majority of the dislocations are confined on basal planes ($\langle a \rangle$ slip systems) as shown in Fig. S4. Clearly, the addition of Ag solute strongly promotes non-basal slip systems in the Mg alloy. The activation of multiple slip systems satisfies the von Mises criterion for homogeneous plastic deformation, and facilitates the formation of dislocation cells. Hence, dislocation cells with an average size of ~100 nm can be achieved in the Mg–Ag alloy as shown in Fig. 1a.

Secondly, segregation of Ag atoms toward dislocation boundaries changed the energy states, structures and misorientations of dislocation boundaries. HAADF-STEM analysis (Fig. 2d) shows that Ag atoms segregate towards the dislocation cell walls during low temperature annealing. Similar segregation behaviors are common in alloy systems with low solubility, such as some of the Fe–Mn and Al alloys [32,34]. Alloying atoms tend to segregate to regions with strong elastic distortions, such as dislocations, dislocation boundaries and GBs. In this work, under the driving force of thermal energy input, segregation of Ag atoms to the dislocation boundaries gradually reduced the local elastic distortions and thus lowered the excess free energy. Sufficient segregation of Ag atoms led to the formation of complexions, which are ordered structural states confined in linear and/or planar regions [32,35,36].

As a part of the restructuring process (formation of complexions), dislocation multiplication and thermally induced dislocation recovery occurred at the dislocation boundaries. Similar to the effect of dislocation interactions under plastic deformation, dislocation multiplication and recovery in the annealed Mg-Ag alloy gradually increased the misorientations of dislocation boundaries and eventually transformed the dislocation boundaries into LAGBs [6,16], as evidenced by the comparable cell sizes and grain sizes (shown in Figs. 1, 2d and 3).

Solute segregation to dislocation boundaries and GBs significantly lowers the migration kinetics of the boundaries, thus can help with stabilizing the microstructures of the materials [34,37–39]. This idea has been adopted to designing stable nanocrystalline alloys [40–42]. It was found that the enthalpy of segregation relative to the enthalpy of mixing in a binary system determines the propensity for segregation stabilization. In this work, Ag segregation occurred during the GB restructuring process. Once the planar complexions are formed along the GBs, the nano-grains became thermally stable. This observation indicates

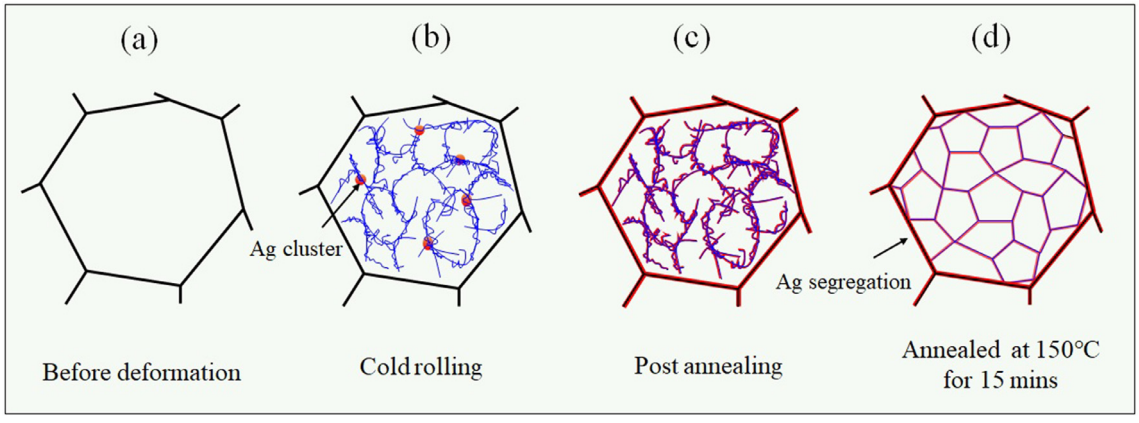

Fig. 4. The schematic diagram of the grain refinement process in Mg–Ag alloy.

that the segregation enthalpy of Ag in Mg solvent satisfies the relationship:

$$\frac{\Delta H_0^{seg}}{(\Delta H^{mix})^a} > c \quad (1)$$

where ΔH_0^{seg} is the enthalpy of boundary segregation and ΔH^{mix} is the enthalpy of mixing; a and c are temperature dependent constants. To date, only a few experimental measurements or atomistic modeling predictions of segregation enthalpies are available. Our work will be an important reference for modeling prediction of the segregation enthalpy in Mg–Ag binary system.

The nanocrystallization process presented in this work has a strict processing sequence as described in Fig. 4. Firstly, a large plastic strain may induce cracks to Mg–Ag alloys [43]. Therefore, the strain input has to be moderate in the cold rolling process. Secondly, Mg–Ag alloys have low melting points and strong propensities for recrystallization at elevated temperatures [44,45]. Therefore, annealing process has to be conducted after a high density of dislocation boundaries were created by cold rolling, for the purpose of boundary transformation and stabilization [46–48]. We did a test on hot rolling of the Mg-Ag sample at 150 °C, whereas the grain sizes were only refined to ~1 μm, as shown in Fig. S5.

In summary, a homogeneously nanocrystalline Mg–Ag alloy is successfully processed by cold rolling and subsequent annealing. During cold rolling, high densities of non-basal dislocations were generated and tangled to form dislocation boundaries/walls. During subsequent annealing, Ag atoms segregated to dislocation boundaries. Multiple reactions including Ag segregation, dislocation multiplication and recovery occurred cooperatively to transform dislocation boundaries into LAGBs. As a result, a unique nanocrystalline structure featured with coarse domains containing nano-grains, have been made in the Mg–Ag alloy. The most salient advantage of the materials processing strategy presented in this work is that only a moderate rolling strain and low annealing temperature are needed; therefore, the strategy has a potential for industrial applications at a low cost.

Declaration of Competing Interest

The authors declare that they have no known competing financial interests or personal relationships that could have appeared to influence the work reported in this paper.

Acknowledgments

This work was supported by the National Key Research and Development Program of China [Grant number: 2017YFB0305501], the National Natural Science Foundation of China [Grant numbers: 51901103, 51931003, 51601003 and 51601094], the Fundamental Research Funds for the Central Universities [Grant number: 30918011342]. The authors wish to express their appreciation to the Jiangsu Key Laboratory of Advanced Micro&Nano Materials and Technology, and the Materials Characterization and Research Center of Nanjing University of Science and Technology. The authors thank S. Pang for materials preparation, Y.F. Liu for calculating dislocation density, and N.N. Liang for TKD experiment.

Supplementary material

Supplementary material associated with this article can be found, in the online version, at doi:10.1016/j.scriptamat.2019.10.012.

References

[1] T.M. Pollock, Science 328 (2010) 986–987.
[2] B.C. Suh, M.S. Shim, K.S. Shin, N.J. Kim, Scr. Mater. 84-85 (2014) 1–6.
[3] W.J. Joost, P.E. Krajewski, Scr. Mater. 128 (2017) 107–112.
[4] R.Z. Valiev, R.K. Islamgaliev, I.V. Alexandrov, Prog. Mater. Sci. 45 (2000) 103–189.
[5] R.Z. Valiev, Y. Estrin, Z. Horita, T.G. Langdon, M.J. Zehetbauer, Y.T. Zhu, JOM 68 (2016) 1216–1226.
[6] Y. Cao, S. Ni, X.L. Liao, M. Song, Y.T. Zhu, Mater. Sci. Eng. R 133 (2018) 1–59.
[7] R.Z. Valiev, Y. Estrin, Z. Horita, T.G. Langdon, M.J. Zehetbauer, Y.T. Zhu, Mater. Res. Lett. 4 (2016) 1–21.
[8] G.J. Raab, R.Z. Valiev, T.C. Lowe, Y.T. Zhu, Mater. Sci. Eng. A 382 (2004) 30–34.
[9] C. Guillemer, M. Clavel, G. Cailletaud, Int. J. Plast. 27 (2011) 2068–2084.
[10] M.H. Yoo, J.R. Morris, K.M. Ho, S.R. Agnew, Metall. Mater. Trans. A 33A (2002) 813–822.
[11] Z.W. Huang, S.B. Jin, H. Zhou, Y.S. Li, Y. Cao, Y.T. Zhu, Int. J. Plast. 112 (2019) 52–67.
[12] W.B. Hutchinson, M.R. Barnett, Scr. Mater. 63 (2010) 737–740.
[13] A. Chapuis, J.H. Driver, Acta Mater. 59 (2011) 1986–1994.
[14] Sean R. Agnew, Özgür Duygulu, Int. J. Plast. 21 (2015) 1161–1193.
[15] K. Hazeli, A. Sadeghi, M.O. Pekguleryuz, A. Kontsos, Mater. Sci. Eng. A 589 (2014) 275–279.
[16] F.J. Humphreys, M. Hatherly, Recrystallization and Related Annealing Phenomena, 2nd ed., Elsevier Ltd, Australia, 2004.
[17] O. Kulyasova, R. Islamgaliev, B. Mingler, M. Zehetbauer, Mater. Sci. Eng. A 503 (2009) 176–180.
[18] P. Liu, S.C. Mao, L.H. Wang, X.D. Han, Z. Zhang, Scr. Mater. 64 (2011) 343–346.
[19] L.H. Wang, X.D. Han, P. Liu, Y.H. Yue, Z. Zhang, E. Ma, Phy. Rev. Lett. 105 (2010) 135501.
[20] K. Eaalati, A. Yamamoto, Z. Horita, T. Ishihara, Scr. Mater. 64 (2011) 880–883.
[21] B. Beausir, S. Biswas, D.I. Kim, L.S. Tóth, S. Suwas, Acta Mater. 57 (2009) 5061–5077.
[22] Y. Liu, X.F. Chen, K. Wei, L.R. Xiao, B. Chen, H.B. Long, Y.D. Yu, Z.H. Hu, H. Zhou, Materials 12 (2019) 1307.
[23] D.B. Williams, C.B. Carter, Transmission Electron Microscopy: A Textbook for Materials Science, 2nd ed., Springer, 2009.
[24] H. Zhou, W.Z. Xu, W.W. Jian, G.M. Cheng, X.L. Ma, W. Guo, S.N. Mathaudhu, Q.D. Wang, Y.T. Zhu, Philos. Mag. 94 (2014) 2403–2409.
[25] X.C. Sha, L.R. Xiao, X.F. Chen, G.M. Cheng, Y.D. Yu, D.D. Yin, H. Zhou, Philos. Mag. 99 (2019) 1957–1969.
[26] W.Z. Xu, Y.F. Zhang, G.M. Cheng, W.W. Jian, P.C. Millett, C.C. Koch, S.N. Mathaudhu, Y.T. Zhu, Nat. Commun. 4 (2013) 2288.
[27] W.Z. Xu, Y.F. Zhang, G.M. Cheng, W.W. Jian, P.C. Millett, C.C. Koch, S.W. Mathaudhu, Y.T. Zhu, Mater. Res. Lett. 2 (2014) 176–183.
[28] S.Q. Zhu, S.P. Ringer, Acta Mater. 144 (2018) 365–375.
[29] Z.Q. Yang, M.F. Chisholm, G. Duscher, X.L. Ma, S.J. Pennycook, Acta Mater. 61 (2013) 350–359.
[30] H. Zhou, G.M. Cheng, X.L. Ma, W.Z. Xu, S.N. Mathaudhu, Q.D. Wang, Y.T. Zhu, Acta Mater. 95 (2015) 20–29.
[31] L.R. Xiao, Y. Cao, S. Li, H. Zhou, X.L. Ma, L. Mao, X.C. Sha, Q.D. Wang, Y.T. Zhu, X.D. Han, Acta Mater. 162 (2019) 214–225.
[32] M. Kuzmina, M. Herbig, D. Ponge, S. Sandlöbes, D. Raabe, Science 349 (2015) 1080–1083.
[33] P.W. Trimby, Y. Cao, Z.B. Chen, S. Han, K.J. Hemker, J.S. Lian, X.Z. Liao, P. Rottmann, S. Samudrala, J.L. Sun, J.T. Wang, J. Wheeler, J.M. Cairney, Acta Mater. 62 (2014) 69–80.
[34] Y. Chen, N. Gao, G. Sha, S.P. Ringer, M.J. Starink, Meter. Sci. Eng. A 627 (2015) 10–20.
[35] M.P. Harmer, Science 332 (2011) 182–183.
[36] S.J. Dillon, M. Tang, W.C. Carter, M.P. Harmer, Acta Mater. 55 (2007) 6208–6218.
[37] P.V. Liddicoat, X.Z. Liao, Y.H. Zhao, Y.T. Zhu, M.Y. Murashkin, E.J. Lavernia, R.Z. Valiev, S.P. Ringer, Nat. Commun. 1 (2010) 63.
[38] R. Kirchheim, Acta Mater. 50 (2002) 413–419.
[39] C.C. Koch, R.O. Scattergood, K.A. Darling, J.E. Semones, J. Mate. Sci. 43 (2008) 7264–7272.
[40] H.A. Murdoch, C.A. Schuh, J. Mater. Res. 28 (2013) 2154–2163.
[41] H.A. Murdoch, C.A. Schuh, Acta Mater. 61 (2013) 2121–2132.
[42] A.R. Kalidindi, C.A. Schuh, Acta Mater. 132 (2017) 128–137.
[43] Z.X. Wu, W.A. Curtin, Nature 526 (2015) 62–67.
[44] H.Q. Sun, Y.-N. Shi, M.-X. Zhang, K. Lu, Acta Mater. 55 (2007) 975–982.
[45] R.X. Zheng, T. Bhattacharjee, A. Shibata, T. Sasaki, K. Hono, M. Joshi, N. Tsuji, Scr. Mater. 131 (2017) 1–5.
[46] T. Chookajorn, H.A. Murdoch, C.A. Schuh, Science 337 (2012) 951–954.
[47] J. Weissmüller, Nanostruct. Mater. 3 (1993) 261–272.
[48] J. Weissmüller, W. Krauss, T. Haubold, R. Birringer, H. Gleiter, Nanostruct. Mater. 1 (1992) 439–447.